Hydrodynamics and microphase ordering in block copolymers: Are hydrodynamics required for ordered phases with periodicity in more than one dimension?

Mark A. Horsch, Zhenli Zhang, and Christopher R. Iacovella
Department of Chemical Engineering, University of Michigan, Ann Arbor, Michigan 48109-2136

Sharon C. Glotzer[a)]
Department of Chemical Engineering, University of Michigan, Ann Arbor, Michigan 48109-2136 and Materials Science Engineering, University of Michigan, Ann Arbor, Michigan 48109-2136

(Received 13 August 2004; accepted 20 September 2004)

We use Brownian dynamics (BD), molecular dynamics, and dissipative particle dynamics to study the phase behavior of diblock copolymer melts and to determine if hydrodynamics is required in the formation of phases with greater than one-dimensional periodicity. We present a phase diagram for diblock copolymers predicted by BD and provide a relationship between the inverse dimensionless temperature ϵ/k_BT and the Flory–Huggins χ parameter, allowing for a quantitative comparison between methods and to mean field predictions. Our results concerning phase behavior are in good qualitative agreement with the theoretical predictions of Matsen and Bates [M. W. Matsen and F. S. Bates, Macromolecules **29**, 1091 (1996)]; however, fluctuation effects arising from finite polymer lengths substantially alter the phase boundaries. Our results pertaining to the hydrodynamics are in contrast to earlier work by Groot *et al.* [R. D. Groot, T. J. Madden, and D. J. Tildesley, J. Chem. Phys. **110**, 9739 (1999); D. Frenkel and B. Smit, *Understanding Molecular Simulation*, 2nd ed. (Academic, New York, 2001)]. In particular, we obtain the hexagonal ordered cylinder phase with BD, a method that does not include hydrodynamics. © *2004 American Institute of Physics*.
[DOI: 10.1063/1.1814976]

I. INTRODUCTION

Increasingly, soft matter is being used to assemble nanobuilding blocks into ordered structures. The ability to manipulate matter on nanometer length scales may be important in future technologies including but not limited to microelectronic applications, magnetic storage and optical devices, drug delivery, and other biomedical applications. Diblock copolymer melts (BCPs) may prove to be particularly useful in the self-assembly of nanobuilding blocks because they themselves self-assemble into complex morphologies such as sheets and cylinders as they attempt to minimize their free energy by aggregating with species of their own kind subject to the topological constraint of being permanently bonded to the incompatible species. This constraint of being bound together limits the distance over which the constituents can separate and therefore provides a method to control the spacing between two or more chemically distinct species. Lopes and co-workers[1] were able to use a polystyrene-block-poly(methyl-methacrylate) template to self-assemble Au, Ag, In, Pb, Sn, and Bi into nanowires due to the metal atoms preferentially favoring one block over the other depending on the metal. Templin and co-workers[2] used the copolymers (3-glycidyloxypropyl-)trimethoxysilane to self-assemble nanoparticles into cylindrical and sheetlike arrays. Computer simulation will play an important role in elucidating trends in the use of soft matter as assemblers of nanobuilding blocks.

In BCPs, phases with one-, two-, and three-dimensional periodicity are observed. Examples are the lamellar phase for one-dimensional periodicity, the hexagonal cylinder phase for two-dimensional periodicity, and the perforated lamellar, gyroid, body centered cubic, and face centered cubic phase for three-dimensional periodicity. In this paper, we test the ability of Brownian dynamics (BD) to predict the correct equilibrium morphologies of linear diblock copolymers and examine the argument proposed by Groot *et al.*[3] that hydrodynamics is required for the formation of the hexagonal cylinder phase. In that, simulations of BCPs using time-dependent Ginzburg–Landau (TDGL) methods without hydrodynamics easily obtain the hexagonal cylinder phase.[4] Here we use BD to map the χN vs f_A phase diagram, where f_A is the relative block fraction of the A component, and then compare the results with the mean field predictions of Matsen and Bates. To date, the phase behavior of BCPs has been studied experimentally,[5] theoretically using self-consistent field theory[6] or mean-field theory,[7,8] and computationally using molecular dynamics (MD),[9,10] discontinuous MD,[11] Monte Carlo (MC),[12,13] dissipative particle dynamics (DPD),[14] and TDGL.[4] It has also been argued that hydrodynamics play a dominant role in the ordering of BCPs, when they form phases with multidimensional periodicity as discussed below. To determine if hydrodynamics are required to form ordered phases with greater than one-dimensional periodicity we compare MD and DPD, which both include hydrodynamics, to BD, which does not include hydrodynamics. One key advantage of BD as compared to mean-field theo-

[a)]Author to whom correspondence should be addressed. Electronic mail: sglotzer@umich.edu

retical methods, lattice MC methods, and DPD is that it readily lends itself to include geometric and topological effects which may be significant in the phase behavior of rigid molecules or nanoparticles attached to flexible molecules such as BCPs, or where the geometry and topology play an important role in the local ordering.[15]

The role of hydrodynamics is not well understood in the ordering of BCPs and it has been predicted through comparison of DPD to BD (Ref. 3) that hydrodynamics are important for the formation of phases with multidimensional periodicity. Specifically, Groot *et al*. reported that BD was unable to form the hexagonally ordered cylinder phase. Since the only difference between the BD and DPD methods used in their study was the hydrodynamic interactions or lack thereof, they concluded that hydrodynamics is required for the formation of the cylinder phase. They further argued that finite size effects were the probable cause as to why MC, which does not include hydrodynamics, was able to form the hexagonal cylinder phase in previous works, as there were only several cylinders contained within the simulation cells studied.[13,16] In work by Horsch *et al*. on polymer-tethered nanoparticles, a hexagonal cylinder phase was found using BD and a different interaction potential than that used by Groot and co-workers, on system sizes with a comparable number of cylinders to the systems they studied. In the Horsch *et al*. system, the tethered particles act somewhat like BCPs due to a thermodynamic immiscibility between tethers and particles and their subsequent tendency to order subject to the topological constraint of being permanently connected. This discrepancy leads to the following question: Is hydrodynamics required for the formation of the cylinder phase in BCPs?

To determine the role of hydrodynamics on microphase ordering and eliminate effects arising from the interaction potentials, we compare MD with a momentum conserving thermostat to BD with a nonmomentum conserving thermostat, with both methods using an identical interaction potential with a $1/r^{12}$ repulsive term. Additionally, we compare DPD with a momentum conserving thermostat to BD with a nonmomentum conserving thermostat, with both methods using an identical interaction potential with an r^2 repulsive term. Comparing methods with identical potentials allows a direct comparison between methods while avoiding complicated mapping of the models being simulated. Throughout the rest of this manuscript we will term the BD used in the MD/BD comparison to be "hard" BD because particles cannot pass through other particles due to the $1/r^{12}$ repulsion, and the BD used in the DPD/BD comparison to be "soft" BD because particles can pass through other particles via an r^2 potential. We also present results pertaining to the phase behavior of the copolymers as a function of relative block fraction f_A and the Flory–Huggins χN parameter as studied by BD with a $1/r^{12}$ repulsive term.

II. MODEL AND METHOD

There are two important features that must be captured in any model of block copolymers. First, the model must incorporate thermodynamic immiscibility between unlike species and second, the model must include connectivity between constituents on the same polymer chain. In all of the studies presented here, the block copolymers are modeled as linear bead-spring chains of N beads with N_A beads of type A and N_B beads of type B. One way to include thermodynamic immiscibility is to use the attractive Lennard-Jones (LJ) interaction potential between like species,

$$\begin{cases} U_{ij}^{\mathrm{LJ}}(r)=4\epsilon_{ij}\left[\left(\dfrac{\sigma}{r_{ij}}\right)^{12}-\left(\dfrac{\sigma}{r_{ij}}\right)^{6}\right]+U_{ij}^{\mathrm{LJ}}(r_c), & r\leqslant r_c \\ U_{ij}^{\mathrm{LJ}}(r)=0, & r>r_c, \end{cases} \tag{2.1}$$

where σ is the diameter of a bead, ϵ_{ij} is the interaction parameter between beads i and j, and the cutoff radius $r_c=2.5\sigma$; and the purely repulsive Weeks-Chandler-Andersen (WCA) interaction potential for unlike species,[17,18]

$$\begin{cases} U_{ij}^{\mathrm{WCA}}(r)=4\epsilon_{ij}\left[\left(\dfrac{\sigma}{r_{ij}}\right)^{12}-\left(\dfrac{\sigma}{r_{ij}}\right)^{6}\right]+\epsilon_{ij}, & r\leqslant r_c \\ U_{ij}^{\mathrm{WCA}}(r)=0, & r>r_c, \end{cases} \tag{2.2}$$

where $r_c=2^{1/6}\sigma$. Here because the potential is truncated at the minimum and shifted up to zero at the r_c the potential is always positive and thus purely repulsive.

The natural units for the LJ systems are σ and ϵ with the time unit $\tau=\sigma\sqrt{m/\epsilon}$, where m is the mass of a bead, $\sigma=\sigma_{AA}=\sigma_{BB}=\sigma_{AB}$ is the diameter of a bead, and $\epsilon=\epsilon_{AA}=\epsilon_{BB}=\epsilon_{AB}$ are the interaction parameters.

Another way to consider thermodynamic immiscibility is to consider only repulsive interactions between species where the repulsion a_{AB} between unlike species is greater than the repulsion a_{AA} between like species.[10,14] An advantage of using purely repulsive interactions is that the cutoff distance is typically small, e.g., 1.0σ, allowing for longer time scales to be realized since fewer forces must be calculated.

In either choice, the connectivity between beads may be modeled as either a finitely extensible nonlinear elastic (FENE) spring or a simple Hookean spring,

$$\begin{aligned} U_{ij}^{\mathrm{FENE}}(r)&=-\frac{1}{2}kR_{\max}^2\ln\left[1-\left(\frac{r_{ij}}{R_{\max}}\right)^2\right], \\ U_{ij}^{\mathrm{harmonic}}(r)&=-\tfrac{1}{2}k(r_{ij})^2, \end{aligned} \tag{2.3}$$

where r_{ij} is the separation between consecutive beads, $R_{\max}=1.5\sigma$ and is the maximum allowable separation between connected beads, and k is the spring constant.

To identify whether hydrodynamic interactions are required for the formation of ordered phases with multidimensional periodicity, we compare MD to hard BD, both with LJ, nonbonded interactions [Eqs. (2.1) and (2.2)], and compare DPD to soft BD, both with purely repulsive quadratic, nonbonded interactions. A summary of the interactions used with each method is given in Table I. In the MD method, Newton's equation of motion is solved for each bead,

$$m\ddot{\mathbf{r}}_i=\mathbf{F}_i, \tag{2.4}$$

where m is the mass of the bead, $\ddot{\mathbf{r}}_i=d^2\mathbf{r}_i/dt^2$, $\mathbf{r}_i$ is the position vector of bead i, and $\mathbf{F}_i$ is the conservative force exerted on bead i by the surrounding beads. A Nose–Hoover

TABLE I. Models used for nonbonded and bonded interactions in the four methods investigated here.

Method	Immiscibility	Connectivity
MD	LJ/WCA	FENE
Hard BD	LJ/WCA	FENE
DPD	$a_{AB}>a_{AA}$	Harmonic
Soft BD	$a_{AB}>a_{AA}$	Harmonic

thermostat is implemented to control the temperature of the system. In the Nose-Hoover scheme, the velocity and time are rescaled at each time step to keep the temperature constant and it has been shown in a study of a binary fluid that hydrodynamic interactions are included.[17] The implementation of the Nose-Hoover thermostat is outlined in Ref. 3.

In the BD method, each bead is subjected to conservative, frictional, and random forces $\mathbf{F}_i^{\mathrm{C}}$, $\mathbf{F}_i^{\mathrm{F}}$, and $\mathbf{F}_i^{\mathrm{R}}$ respectively, and obeys the following equation of motion:[19]

$$m\ddot{\mathbf{r}}_i=\mathbf{F}_i^{\mathrm{C}}+\mathbf{F}_i^{\mathrm{F}}+\mathbf{F}_i^{\mathrm{R}}. \tag{2.5}$$

The frictional force acts as a heat sink and is calculated using Stokes' law relation $\mathbf{F}_i^{\mathrm{F}}=-\zeta\mathbf{v}_i=-6\pi a\,\eta\mathbf{v}_i$, where ζ is the friction coefficient, a is the bead radius, η is the viscosity, and $\mathbf{v}_i$ is the bead velocity. The random force $\mathbf{F}_i^{\mathrm{R}}$ acts as a heat source and is calculated using the fluctuation dissipation theorem,[10]

$$\langle\mathbf{F}_i^{\mathrm{R}}(t)\mathbf{F}_j^{\mathrm{R}}(t')\rangle=6k_{\mathrm{B}}Tm\zeta\delta_{ij}\delta(t-t'). \tag{2.6}$$

Together the frictional and random forces act as a nonmomentum conserving thermostat[20] and, therefore, for large enough ζ, hydrodynamic interactions are not included in BD. In this study, we vary ζ between $0.5m\tau^{-1}$ and $5.0m\tau^{-1}$. For these values we ran BD simulations of an A/B binary mixture with the same interaction potentials used for the BCPs, and observed late stage coarsening with an exponent of 1/3. This value indicates the coarsening is diffusive,[21] and thus hydrodynamics are suppressed with the values of ζ that we use.

In the DPD method, unlike the previously discussed methods, beads are treated as fluid elements rather than hard particles. That is, the beads are soft and can pass through each other allowing for large time steps and thus longer timescales to be realized. As in the BD method, beads in the DPD simulation are also subjected to conservative, frictional, and random forces $\mathbf{F}_i^{\mathrm{C}}$, $\mathbf{F}_i^{\mathrm{F}}$, and $\mathbf{F}_i^{\mathrm{R}}$, respectively, and subsequently their trajectories are governed by Eq. (2.5). However, unlike in BD both the random and frictional forces act in a pairwise manner and thus obey Newton's third law, conserve momentum, and include hydrodynamics. Details of this method can be found in Refs. 22 and 23. In the DPD simulations the conservative force is purely repulsive and is given by

$$\mathbf{F}_{ij}^{\mathrm{C}}=\begin{cases}a_{ij}(1-r_{ij})\hat{\mathbf{r}}_{ij}, & r_{ij}<1\\ 0, & r_{ij}\geqslant 1,\end{cases} \tag{2.7}$$

where a_{ij} is the maximum repulsion between beads i and j, r_{ij} is the distance between the beads, and $\hat{\mathbf{r}}_{ij}$ is a unit vector in the direction of the line of centers between beads i and j. We use similar parameters as Groot *et al.*,[14] for like species, $a_{ij}=a_{AA}=a_{BB}=25k_{\mathrm{B}}T$ and for unlike species, $a_{ij}=a_{AB}=a_{AA}+3.27\chi$, for $\rho=3$. The natural units of the DPD and soft BD systems are $r_c=1.0\sigma$ and $k_{\mathrm{B}}T$ with the time unit $\tau=r_c\sqrt{m/k_{\mathrm{B}}T}$, where m is the mass of a bead.

All simulations are initially carried out in a cubic cell with periodic boundary conditions. The time step Δt used to integrate the discretized equations of motion is chosen to be $\Delta t=0.01\tau$ for the MD/hard BD comparison and 0.04τ for the DPD/soft BD comparison. The number density of the MD/hard BD simulations is $\rho=0.85\sigma^{-3}$ and for the DPD/soft BD simulations the number density is $\rho=3r_c^{-3}$. Systems are equilibrated at effectively infinite temperature $\epsilon=0$ and subsequently cooled to the target temperature in the microphase-separated region.

III. MAPPING TO FLORY–HUGGINS PARAMETER

In order to compare the same state points among different methods and also to compare the results to mean-field predictions we determined the relationship between the inverse dimensionless, system temperature, and the Flory–Huggins χ parameter. Groot *et al.* provide this relationship for the DPD and soft BD methods used[23] in our simulations. Below we briefly outline the development of this relationship between $\epsilon/k_{\mathrm{B}}T$ and χ for the MD and hard BD methods, which closely follows the work by Groot and co-workers. The general Flory–Huggins free energy expression for a two-component polymer mixture is

$$\frac{F}{K_{\mathrm{B}}T}=\frac{f_A}{N_A}\ln f_A+\frac{1-f_A}{N_B}\ln(1-f_A)+\chi f_A(1-f_A), \tag{3.1}$$

where f_A and f_B are the volume fractions (also the block fractions as in a BCP blend) and N_A and N_B are the number of beads in each A and B block. For a symmetric system ($N_A=N_B$) the free energy is minimized at a value of χN_A given by[23]

$$\chi N_A=\frac{\ln[(1-f_A)/f_A]}{1-2f_A}. \tag{3.2}$$

To determine the relative solubility between species A and B, we set up a simulation box of $\sim 12.3\sigma\times 12.3\sigma\times 45\sigma$ which corresponds to roughly 6000 monomers where half the monomers are of type A and the system density $\rho=0.85\sigma^{-3}$. The initial configuration for this determination is such that all the A type monomers are contained in one half of the box and the B type in the other half, thus creating an interface between the different monomer types. A value for $\epsilon/k_{\mathrm{B}}T$ is chosen and the simulation is run until the potential energy reaches a steady state. At that point, data is saved for $\approx 10^6$ time steps and the concentration profile is averaged. The concentration profile is then plotted as a function of the x coordinate, the long dimension of the simulation cell, and the value of the concentration corresponding to the region of constant concentration is inserted into Eq. (3.2) (see Fig. 1 for a representative concentration profile). A value of χ is then calculated. Note the value for N_A is unity for single beads, as used for this excercise. This procedure is per-

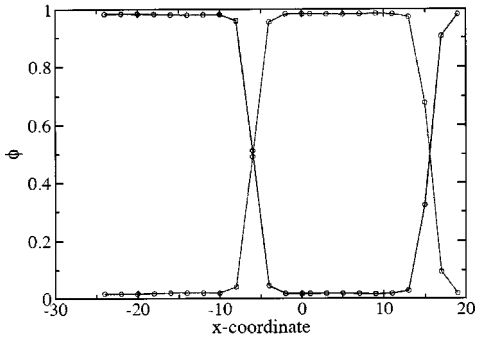

FIG. 1. Concentration profile of A/B monomer mixture as a function of the x coordinate in a simulation cell of $12.3\sigma\times12.3\sigma\times45\sigma$ with $N=5760$, $\rho=0.85\sigma^{-3}$, $\epsilon/k_BT=0.5$, and $t\sim10^5\tau$.

formed for several other values of ϵ/k_BT and the results plotted, providing a relationship between ϵ/k_BT and χ (Fig. 2).

We find there is a linear relationship between the energy parameter and the Flory–Huggins parameter given explicitly by

$$\chi N=[9.48(\pm0.11)\epsilon/k_BT-0.09]N. \tag{3.3}$$

However, because we are simulating rather small polymers it is necessary to account for the effects of fluctuations in the chain length. We use the Ginsburg parameter[5] $\bar{N}=6^3(R_g^3\rho_{BCP})^2$ to calculate the effective polymer length, where R_g is the radius of gyration and ρ_{BCP} is the BCP number density. Fredrickson and Helfand predicted that the order-disorder transition (ODT) for finite length polymer chains is given by

$$(\chi N)_{ODT}=10.5+\bar{N}^{-1/3}. \tag{3.4}$$

Since the above equation assumes that R_g scales as the number of statistical segments to the one-half power, we must apply the correct scaling. By performing several runs with polymer lengths ranging from $N=5$ to $N=10$ we see that $R_g\sim N^v$, where v is 0.69. This scaling, along with the weak coupling calculations of Fredrickson and Helfand and the Ginsburg parameter, results in the following effective Flory–Huggins parameter $(\chi N)_{eff}$:[14]

$$(\chi N)_{eff}\approx\frac{\chi N}{1+3.9N^{-0.71}}. \tag{3.5}$$

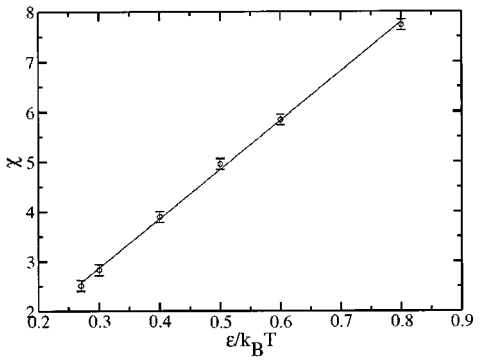

FIG. 2. χ vs ϵ/k_BT mapping for A/B monomer mixture.

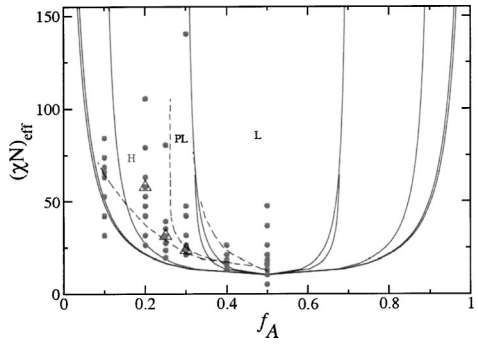

FIG. 3. Phase diagram of a block copolymer melt obtained via hard BD simulations for $\rho=0.85\sigma^{-3}$ (see Table I). Simulated state points from hard BD are filled circles, the dashed lines are the predicted phase boundaries, solid lines represent the phase diagram as predicted by Matsen and Bates for infinite length polymer chains, and the unfilled triangles are state points predicted using MD.

Inserting Eq. (3.3) into Eq. (3.5) provides a relationship between ϵ/k_BT and the effective Flory–Huggins parameter that takes into account the small chain lengths used in our simulations,

$$(\chi N)_{eff}\approx\frac{[(9.48\pm0.11)\epsilon/kT-0.09]N}{1+3.9N^{-0.71}}. \tag{3.6}$$

Equation (3.6) allows for a quantitative comparison between our simulation results and the Matsen and Bates phase diagram,[24] which was calculated using mean-field theory.

For the DPD and soft BD simulations we used the mapping determined by Groot and co-workers,

$$(\chi N)_{eff}\approx\frac{(a_{AB}-a_{AA})(0.306\pm0.003)N}{1+3.9N^{-0.51}}. \tag{3.7}$$

IV. RESULTS AND DISCUSSION

For BCP melts we examine two issues. First, we address the phase behavior as a function of χN and block fraction f_A. Here BD is used to map the phase diagram of diblock copolymers. Second, we address the role of hydrodynamics to determine whether hydrodynamics is required for the formation of the hexagonally ordered cylinder phase.

Using hard BD, we studied both symmetric and asymmetric block copolymers for relative block fractions of $f_A=0.1$, 0.2, 0.25, 0.3, 0.4, and 0.5 and observed disordered micelle "*M*," hexagonally ordered cylinder "*H*," perforated lamellar "PL," and lamellar "*L*" phases (see Fig. 3). When we account for fluctuation effects due to the small polymer size, we find that for symmetric copolymers the order-disorder transition occurs at a value of $(\chi N)_{ODT}$ of roughly (11.37 ± 0.9), slightly higher than $\chi N=10.5$ predicted by Leibler[8] using mean-field theory. However, the difference between the theoretical and computational values falls within the error of the χ mapping to ϵ/k_BT. For symmetric block copolymers A_5B_5 ($f_A=0.5$) only the lamellar phase is observed for values of $(\chi N)_{eff}$ greater than the ODT temperature, as predicted by Leibler.[8] An example of the lamellar morphology for $(\chi N)_{eff}=52.7$ is shown in Fig. 4(a). As we increase the degree of asymmetry in the BCPs, we see the

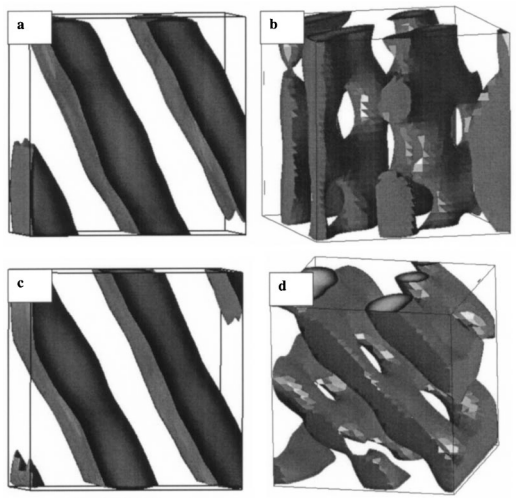

FIG. 4. Lamellar and perforated lamellar phases obtained via MD and hard BD simulations with $N=8000$ and $\rho=0.85\sigma^{-3}$. (a) Lamellar phase obtained using hard BD with $(\chi N)_{\text{eff}}=52.7$, $f_A=0.5$, and $t=6000\tau$. (b) Perforated lamellar phase obtained using hard BD with $(\chi N)_{\text{eff}}=21.1$, $f_A=0.4$, and $t=21\,000\tau$. (c) Lamellar phase obtained using MD with $(\chi N)_{\text{eff}}=52.7$, $f_A=0.5$, and $t=9000\tau$. (d) Perforated lamellar phase obtained using MD with $(\chi N)_{\text{eff}}=21.1$, $f_A=0.4$, and $t=18\,000\tau$.

development of the perforated lamellar phase for values of $f_A=0.4$ and 0.3 where increasing asymmetry requires decreasing the temperature to stay within this phase. The PL morphology obtained at $(\chi N)_{\text{eff}}=21.1$ and $f_A=0.4$ is shown in Fig. 4(b). To facilitate the formation of equilibrium structures with multidimensional periodicity such as the PL phases, sequential cooling is applied in the simulation, see Fig. 5(a) for an example of one cooling curve. This is different from the symmetric BCPs that form only the lamellar

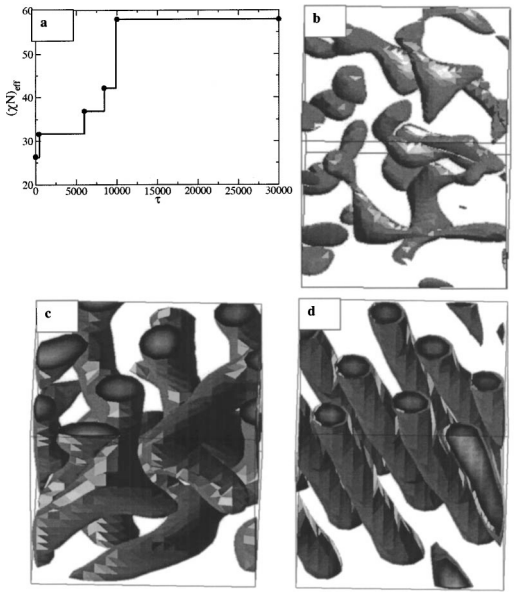

FIG. 5. Morphological evolution for hexagonal cylinder phase obtained with hard BD simulation, $N=13\,000$ and $\rho=0.85\sigma^{-3}$. (a) Cooling schedule from high temperature to target temperature (b) disordered state, $(\chi N)_{\text{eff}}=36.8$, $f_A=0.2$, and $t=7000\tau$. (c) Interconnected tube structure, $(\chi N)_{\text{eff}}=57.9$, $f_A=0.2$, and $t=10\,900\tau$. (d) Hexagonal cylinder structure at $(\chi N)_{\text{eff}}=57.9$, $f_A=0.2$, and $t=30\,000\tau$.

phase when quenched directly from a disordered state to the target $(\chi N)_{\text{eff}}$. It is not entirely clear if the PL phase is a stable phase[25] or if this phase is stabilized from the gyroid phase by the finite simulation size. Neither self-consistent nor mean-field theories predict the PL phase; however, it has been experimentally observed[26] and has been predicted by other computational works.[11,14] As we further increase the asymmetry, for a fixed value of $(\chi N)_{\text{eff}}$, we see the formation of hexagonally packed cylinders at $f_A=0.1$, 0.2, 0.25, and 0.3. The morphological evolution of the system as it is cooled from $(\chi N)_{\text{eff}}=36.8$ to $(\chi N)_{\text{eff}}=57.9$ for $f_A=0.2$ is shown in Fig. 5. [The corresponding cooling process is shown in Fig. 5(a).] As still more asymmetry is introduced for a given $(\chi N)_{\text{eff}}$, we see the formation of disordered *M*. We compare the phase diagram obtained by hard BD to those of Schultz *et al.*,[11] where they used discontinuous molecular dynamics and a box search algorithm to study block copolymer phase behavior, and find good qualitative agreement with their studies, noting that we also find the *L*, PL, and *H* phases for block copolymers of length $N=10$ for a volume fraction of $\phi=0.45$. However, we see a narrower PL region and a broadened hexagonal cylinder phase. Compared with the mean-field theoretical predictions of Matsen and Bates we find that the cylinder phase is shifted to more asymmetric block fractions and is broader. We note that we observe no bcc and fcc cubic micelle phases. The absence of these phases are likely a result of the small polymer lengths used in the simulations. Here the fluctuations in polymer length may be too great to observe phases that have been predicted by mean-field theory to exist in only a very narrow window of the phase diagram. Schultz *et al*. also did not observe, for short polymers of $N=10$, bcc and fcc phases but for polymers of length $N=20$ they observed the bcc phase.

To avoid metastable structures due to local minima trapping, we ran several simulations each starting from a different initial configuration and for several different box sizes as well. Specifically, we ran nine independent simulations for $f_{\text{A}}=0.5$, seven independent simulations for $f_{\text{A}}=0.2$ and $f_{\text{A}}=0.3$, and four independent simulations for $f_{\text{A}}=0.25$ and $f_{\text{A}}=0.4$, all for $N=8000$. We also simulated systems of $N=8000$, 13 000, and 20 000 for $f_{\text{A}}=0.2$, 0.3, and 0.4 as these are regions with multidimensional periodicity. The periodic spacing of the equilibrated structures and the potential energy per bead were then compared for the hexagonal cylinder phase for $f_{\text{A}}=0.2$, and $N=8000$, 13 000, and 20 000, see Table II. We further ran three simulations using the box search algorithm (described below) for $f_{\text{A}}=0.2$ and $N=8000$, for a noncubic simulation cell of $18.0\sigma\times18.2\sigma\times28.7\sigma$, and calculated the periodic spacing and the energy. The periodic spacing and the potential energy per bead is statistically the same for each of these systems and is summarized in Table II. To calculate the periodic spacing between cylinders we find a vector equation of the form $\mathbf{x}=\mathbf{b}+c\mathbf{r}$ for each cylinder, where $\mathbf{x}$ is the vector passing through point $\mathbf{b}$, a point that lies in the cylinder, c is a scalar and can take on any value, and $\mathbf{r}$ is a vector describing the direction of the cylindrical axis. We then calculated the distance between all beads in a specific cylinder and all beads within its

TABLE II. Spacing between cylinders for hexagonal cylinder phase obtained using hard BD with $f_A=0.2$. $(\chi N)_{\text{eff}}$ is the effective Flory-Huggins parameter, N is the number of beads, d is the spacing between cylinders in units of σ, and the potential energy per bead is in units of k_BT.

Simulation cell	$(\chi N)_{\text{eff}}$	N	$d(\sigma)$	Energy $(k_BT)/N$
Cubic	57.9	8 000	8.64±0.3	13.77±0.04
Cubic	57.9	13 000	8.63±0.32	13.75±0.06
Cubic	57.9	20 000	8.57±0.2	13.77±0.02
Noncubic	57.9	8 000	8.62±0.19	13.78±0.01

neighboring cylinders using the following expression for the distance between a point and a line:

$$d=\frac{|(\mathbf{x}_2-\mathbf{x}_1)\times(\mathbf{x}_1-\mathbf{x}_0)|}{|(\mathbf{x}_2-\mathbf{x}_1)|}, \tag{4.0}$$

where d is the distance between any point and the line describing the cylindrical axis, $\mathbf{x}_2$ and $\mathbf{x}_1$ are points on the line describing the cylindrical axis, and $\mathbf{x}_0$ is the position of the bead. The distances are then averaged over all beads within the two cylinders being tested and the average value of the spacing between all neighboring cylinders is then the periodic spacing between cylinders.

The box search algorithm used here was developed by Schultz *et al.*[27] and allows the simulation cell to change the relative length of the rectilinear coordinate axis based on the internal pressure. The box search algorithm seeks to minimize free energy subject to the constraint of constant volume. Note that in the noncubic cell the cylinders are parallel to the coordinate axis. The above tests provide strong supporting evidence that our systems are large enough to avoid finite size effects pertaining to the equilibrium morphology; however, we cannot conclusively argue that there are no finite size effects on the dynamical process. We can argue, however, that our systems are of the same size or larger than those of Groot and co-workers in the number of cylinders formed within a simulation cell and that in contrast to their work we see the formation of the hexagonal cylinder phase for methods that exclude hydrodynamics.

To further investigate the role of hydrodynamics, we compare the hard BD results to the MD results. We see that for the same parameters the morphological evolution from the disordered state to hexagonally packed cylinders is essentially the same for both the hard BD and MD simulations as shown in Figs. 5 and 6. In particular, both pass through an interconnected tube state before finally forming the hexagonal cylinder phase. The results for several simulations at different values of $(\chi N)_{\text{eff}}$ and f_A are listed in Table III and are shown for MD as different symbols in Fig. 3. We see from Table III and Figs. 3, 4, 5, and 6 that for the same conditions MD and hard BD both produce the same final structure irrespective of the presence or absence of hydrodynamic interactions.

To ensure that our findings for the MD and hard BD are not dependent on the interaction potential we now compare the results of DPD and soft BD simulations. Again for $f_A=0.2$, 0.25, and 0.3 we see the formation of the hexagonal cylinder phase at $(\chi N)_{\text{eff}}=57.9$, $(\chi N)_{\text{eff}}=31.4$, $(\chi N)_{\text{eff}}=23.7$, respectively, for the DPD method. Again we observe the evolution from a disordered state to a transient connected tube state, and then finally the formation of the hexagonal cylinder phase. Figures 7(a) and 7(b) shows examples of the interconnected tube state and the hexagonal cylinder phase. For the DPD systems we performed three independent simulations for system sizes of $N=8000$, 13 824, and 27 000 for each $(\chi N)_{\text{eff}}$ listed in Table III. We then ran identical systems in the soft BD simulations and again find the formation of the hexagonal cylinder phase. Here we also observe the evolution from a disordered state to the interconnected tube state, and finally the evolution to hexagonal cylinders see Figs. 7(c) and 7(d). We also point out that the number of cylinders in the largest DPD and soft BD simulations is approximately the same number of cylinders as in the $N=13\,000$ bead systems simulated using MD and hard BD, and that these are very similar to the system sizes reported in the work by Groot. To this extent we demonstrate the formation of the hexagonal cylinder phase for methods that possess or lack hydrodynamic interactions for two different interaction potentials. Our observations do not, however, explain

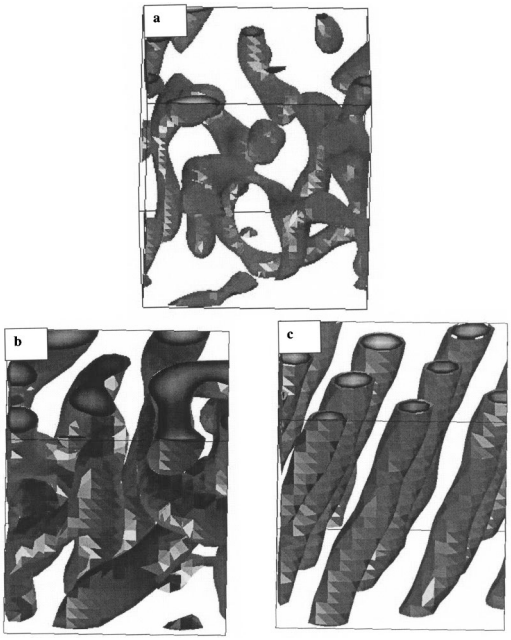

FIG. 6. Morphological evolution of hexagonal cylinder phase obtained with MD simulation, $N=13\,000$ and $\rho=0.85\sigma^{-3}$. The cooling schedule is the same as Fig. 5(a). (a) Disordered state, $(\chi N)_{\text{eff}}=36.8$, $f_A=0.2$, and $t=7000\tau$. (b) Interconnected tube structure, $(\chi N)_{\text{eff}}=57.9$, $f_A=0.2$, and $t=10\,000\tau$. (c) Hexagonal cylinder structure at $(\chi N)_{\text{eff}}=57.9$, $f_A=0.2$, and $t=30\,000\tau$.

TABLE III. System parameters and phase morphology for comparison between MD and hard BD and between DPD and soft BD. $(\chi N)_{\text{eff}}$ is the effective Flory-Huggins parameter, N_b is the polymer length, Δt is the time step, t the simulation time where τ is the simulation time unit, and f_A is the relative block fraction (or, equivalently, volume fraction) of species A.

Method	$(\chi N)_{\text{eff}}$	N_b	N	Δt^*	t	f_A	Phase
MD	57.9	10	13 000	0.01	$\sim 10^4\tau$	0.2	hex cyl
MD	31.4	8	13 000	0.01	$\sim 10^4\tau$	0.25	hex cyl
MD	23.7	10	13 000	0.01	$3.0\times 10^4\tau$	0.3	hex cyl
Hard BD	57.9	10	13 000	0.01	$\sim 10^4\tau$	0.2	hex cyl
Hard BD	31.4	8	13 000	0.01	$\sim 10^4\tau$	0.25	hex cyl
Hard BD	23.7	10	13 000	0.01	$3.0\times 10^4\tau$	0.3	hex cyl
DPD	57.9	10	27 000	0.04	$\sim 10^4\tau$	0.2	hex cyl
DPD	31.4	8	13 824	0.04	$\sim 10^4\tau$	0.25	hex cyl
DPD	23.7	10	27 000	0.04	$3.0\times 10^4\tau$	0.3	hex cyl
Soft BD	57.9	10	27 000	0.04	$\sim 10^4\tau$	0.2	hex cyl
Soft BD	31.4	8	13 824	0.04	$\sim 10^4\tau$	0.25	hex cyl
Soft BD	23.7	10	27 000	0.04	$1.5\times 10^5\tau$	0.3	hex cyl

why our results differ from those of Groot *et al.*,[3] who were unable to obtain cylinders with soft BD. One possibility is that our friction coefficient while large enough to suppress hydrodynamics in late-stage coarsening of a mixture, is small enough that a flow field persists on the length scale of the periodic spacing between cylinders. However, since the friction coefficient used in our study is larger than that used in the Groot study, our flow field should have a smaller characteristic length, and consequently even less of a hydrodynamic contribution. We can therefore confidently rule this out as the cause of the discrepancy. Thus we conclude that the observed hexagonal cylinder phase is robust and that hydrodynamic interactions are not required for the formation of phases such as the hexagonal cylinder phase with greater than one-dimensional periodicity.

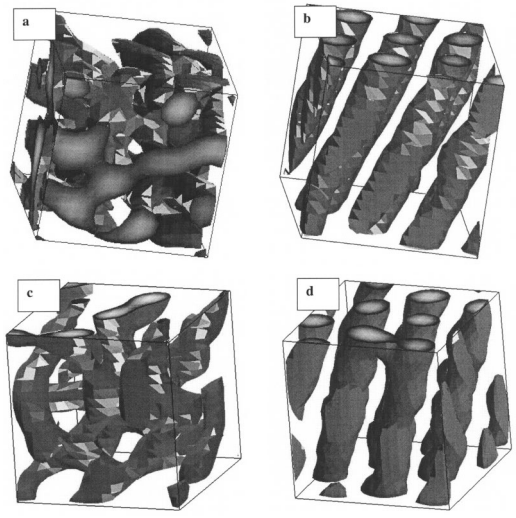

FIG. 7. Morphological evolution of hexagonal cylinder phase obtained using DPD and soft BD simulations with $N=27\,000$, $f_A=0.3$, and $\rho=3.0r_c^{-3}$. (a) Interconnected tube structure obtained using DPD with $t=1000\tau$ and $(\chi N)_{\text{eff}}=23.7$. (b) Hexagonal cylinder phase obtained using DPD with $t=30\,000\tau$ and $(\chi N)_{\text{eff}}=23.7$. (c) Interconnected tube structure obtained using soft BD with $t=1000\tau$ and $(\chi N)_{\text{eff}}=23.7$. (d) Hexagonal cylinder phase obtained using soft BD with $t=150\,000\tau$ and $(\chi N)_{\text{eff}}=23.7$.

Finally, we note that, upon comparing MD to hard BD, we observed no appreciable difference in the number of time steps required for the formation of the hexagonal cylinder phase. This was also true for the DPD/soft BD comparison for $f_A=0.2$ and 0.25. However, for the three independent runs performed for $f_A=0.3$ and $N=27\,000$, in the DPD/soft BD comparison, we observed the longest time required for the formation of the hexagonal cylinder phase using DPD to be $30\,000\tau$, while for soft BD we saw the formation of the hexagonal cylinder phase at $80\,000\tau$, $140\,000\tau$, and $150\,000\tau$. While a detailed comparison of the relative efficiency of these methods is outside the scope of the present work, this may provide some useful information.

V. CONCLUSIONS

We performed MD, hard BD, soft BD, and DPD simulations of a BCP melt and have investigated the χN vs f_A phase behavior and the role of hydrodynamics in the microphase ordering process. Our BCP phase diagram is predicted using hard BD or MD and is in good qualitative agreement with those predicted by Schultz *et al.* using hard spheres. We find the $(\chi N)_{\text{ODT}}$ to be in good quantitative agreement, within error, to the theoretical predictions of Leibler when we adjust for finite chain lengths. Also, the order-order transitions are in good qualitative agreement with theory but are quantitatively different. We note the absence of the gyroid phase and the presence of the perforated lamellar phase in regions where the gyroid phase may be anticipated. The reason for these differences most likely lies in the relatively short polymers used in this study as the theoretical predictions are for infinite length polymers.

We developed a relationship between the Flory–Huggins parameter χN and the LJ parameter ϵ/k_BT and directly compared MD, which includes hydrodynamics, to hard BD, which does not include hydrodynamics for the same χN value. We saw the formation of an interconnected tube state *en* route to the hexagonal cylinder phase that was realized by both methods irrespective of the inclusion or lack of hydrodynamics. We also note that both methods produced the perforated lamellar phase further demonstrating that hydrody-

namics is not required for the formation of phases with periodicity in more than one dimension. Further we compared DPD to soft BD and again found that both methods formed an interconnected tube state *en* route to the formation of the hexagonal cylinder phase, with or without hydrodynamics, demonstrating that the ability of the hard BD system to form the hexagonal cylinder phase is robust.

ACKNOWLEDGMENTS

Financial support was provided by the U.S. Department of Energy, Grant No. DE-FG02-02ER46000. The authors thank the National Partnership for Advanced Computational Infrastructure (NPACI) and the University of Michigan Center for Advanced Computing for CPU time. The authors are grateful to Ron G. Larson for a critical reading of the manuscript, and Daan Frenkel and Patrick B. Warren for helpful discussions.

[1] W. A. Lopes and H. M. Jaeger, Nature (London) **414**, 735 (2001).
[2] M. Templin, A. Franck, A. DuChesne, H. Leist, Y. M. Zhang, R. Ulrich, V. Schadler, and U. Wiesner, Science **278**, 1795 (1997).
[3] R. D. Groot, T. J. Madden, and D. J. Tildesley, J. Chem. Phys. **110**, 9739 (1999); D. Frenkel and B. Smit, *Understanding Molecular Simulation,* 2nd ed. (Academic, New York, 2001).
[4] S. Y. Qi and Z. G. Wang, Phys. Rev. E **55**, 1682 (1997).
[5] F. S. Bates and G. H. Fredrickson, Annu. Rev. Phys. Chem. **41**, 525 (1990).
[6] M. W. Matsen and F. S. Bates, J. Polym. Sci., Part B: Polym. Phys. **35**, 945 (1997); M. W. Matsen and M. Schick, Phys. Rev. Lett. **72**, 2660 (1994).
[7] G. H. Fredrickson and E. Helfand, J. Chem. Phys. **87**, 697 (1987).
[8] L. Leibler, Macromolecules **13**, 1602 (1980).
[9] M. Murat, G. S. Grest, and K. Kremer, Macromolecules **32**, 595 (1999).
[10] G. S. Grest, M. D. Lacasse, K. Kremer, and A. M. Gupta, J. Chem. Phys. **105**, 10583 (1996).
[11] A. J. Schultz, C. K. Hall, and J. Genzer, J. Chem. Phys. **117**, 10329 (2002).
[12] G. Besold, O. Hassager, and O. G. Mouritsen, Comput. Phys. Commun. **122**, 542 (1999); A. Hoffmann, J. U. Sommer, and A. Blumen, J. Chem. Phys. **106**, 6709 (1997); R. G. Larson, Macromolecules **27**, 4198 (1994).
[13] A. Hoffmann, J. U. Sommer, and A. Blumen, J. Chem. Phys. **107**, 7559 (1997); R. G. Larson, *ibid*. **96**, 7904 (1992).
[14] R. D. Groot and T. J. Madden, J. Chem. Phys. **108**, 8713 (1998).
[15] Z. L. Zhang, M. A. Horsch, M. H. Lamm, and S. C. Glotzer, Nano Lett. **3**, 1341 (2003).
[16] K. Binder and H. Fried, Macromolecules **26**, 6878 (1993).
[17] M. Laradji, S. Toxvaerd, and O. G. Mouritsen, Phys. Rev. Lett. **77**, 2253 (1996).
[18] R. Yamamoto and X. C. Zeng, Phys. Rev. E **59**, 3223 (1999).
[19] G. S. Grest and K. Kremer, Phys. Rev. A **33**, 3628 (1986).
[20] K. Kremer and G. S. Grest, J. Chem. Phys. **92**, 5057 (1990).
[21] J. D. Gunton, M. San Miguel, and P. S. Sahni, *Phase Transitions and Critical Phenomena* (Academic, New York, 1983); E. D. Siggia, Phys. Rev. A **20**, 595 (1979).
[22] P. Espanol and P. Warren, Europhys. Lett. **30**, 191 (1995); P. J. Hoogerbrugge and J. Koelman, *ibid*. **19**, 155 (1992).
[23] R. D. Groot and P. B. Warren, J. Chem. Phys. **107**, 4423 (1997).
[24] M. W. Matsen and F. S. Bates, Macromolecules **29**, 1091 (1996).
[25] H. Hasegawa, Curr. Opin. Colloid Interface Sci. **3**, 264 (1998).
[26] A. K. Khandpur, S. Forster, F. S. Bates, I. W. Hamley, A. J. Ryan, W. Bras, K. Almdal, and K. Mortensen, Macromolecules **28**, 8796 (1995); K. Almdal, K. A. Koppi, F. S. Bates, and K. Mortensen, *ibid*. **25**, 1743 (1992).
[27] A. J. Schultz, C. K. Hall, and J. Genzer, J. Chem. Phys. **120**, 2049 (2004).